King Saud University

Arabian Journal of Chemistry

www.ksu.edu.sa
www.sciencedirect.com

ORIGINAL ARTICLE

The mechanism of ultrasound oxidation effect on the pyrite for refractory gold ore pretreatment

Qihao Gui [a,b], Shixing Wang [a,b,c,*], Libo Zhang [a,b,c,*]

[a] *Faculty of Metallurgical and Energy Engineering, Kunming University of Science and Technology, Kunming, Yunnan 650093, China*
[b] *State Key Laboratory of Complex Nonferrous Metal Resources Clean Utilization Kunming University of Science and Technology, Kunming, Yunnan 650093 China*
[c] *National Local Joint Laboratory of Engineering Application of Microwave Energy and Equipment Technology, Kunming, Yunnan 650093, China*

Abstract The effect of ultrasonic cavitation on the oxidation of the crystal pyrite in deionized water has been discussed. The effect of solution alkalinity, ultrasonic power and temperature on the surface morphology of pyrite and the chemical forms of sulfur and iron was discussed. The surface of pyrite is severely corroded under ultrasound. The sulfur in the pyrite is oxidized to $S_2O_3^{2-}$ and SO_4^{2-}. Most of the iron is in the form of Fe^{2+}, few of it is in the form of Fe^{3+}. With the increase of alkalinity, ultrasonic power and temperature, the surface corrosion of pyrite becomes more and more obvious. With the increase of the NaOH concentration, the Fe(II) concentration in solution decreases and the deposition of iron oxides on the pyrite surface prevents pyrite oxidation. With the increase of the ultrasonic power, the Fe(II) concentration in solution increase. The effect of the NaOH concentration on the SO_4^{2-} and $S_2O_3^{2-}$ concentration indicates pyrite oxidation is in mild alkalinity under ultrasound. The concentration of SO_4^{2-} and $S_2O_3^{2-}$ increases along with increase of the ultrasonic power and decreases tremendously with increase of the temperature. The pyrite oxidation is initiated by hydroxyl radical and promoted by Fe^{3+}.

© 2021 The Author(s). Published by Elsevier B.V. on behalf of King Saud University. This is an open access article under the CC BY-NC-ND license (http://creativecommons.org/licenses/by-nc-nd/4.0/).

1. Introduction

Pyrite is the main inclusion in refractory gold ore, which complicated the gold extraction process significantly (Fraser et al., 1991). Several methods are proposed to open the inclusion (Boboev et al., 2016; Fomchenko, 2016; Li et al., 2009). Roasting and chemical oxidation is the most common method. Liu *et al.* applied Na_2SO_4 assisted roasting to remove sulfur and arsenic (Liu et al., 2019). Moreover, the addition of Na_2SO_4 effectively increases the sintering rate and the solubility of roasting slag. Ofori-Sarpong *et al.* used fungus to oxidized sul-

fide (pyrite, arsenopyrite, etc.) (Ofori-Sarpong et al., 2011). After the gold inclusions were oxidized by the fungus, the gold was exposed or the inclusion was converted into porous oxides, thereby achieving the purpose of the increasing gold leaching rate. Alkaline sulfide leaching pretreatment could effectively remove antimony, which could form insoluble antimonate and hinder the dissolution of gold (Celep et al., 2011; Deschênes et al., 2009). The main purpose of these pretreatments is to open the inclusion and expose the enclosed gold.

As a mechanical wave with high energy density, ultrasound has been applied in many industrial fields recent years (Šíma et al., 2009; Xin et al., 2013; Luque-García and Luque de Castro, 2003; Verdan et al., 2003; Zhang et al., 2016). The intensive ultrasound could induce cavitation, which brings high temperature and high pressure with high frequency particle vibration. The cavitation extensively intensifies the chemical process (Rooze et al., 2013; Ishihara et al., 1975; Feng et al., 2002; Shchukin et al., 2011; Wang et al., 2014). In our previous studies, the introduction of ultrasound in alkaline solution during the pretreatment stage of gold ore significantly increases the leaching rate of gold from refractory ore (Zhang et al., 2016). Though the application of ultrasound rises great attention in recent year, but few researches are focus on the mechanism of ultrasound action. Therefore, the mechanism of how the ultrasounds open the inclusions and increase the gold leaching rate needs to be explained.

In the work, the effect of ultrasonic cavitation on the oxidation of the crystal pyrite in deionized water has been discussed. The effect of solution alkalinity, ultrasonic power and temperature on the surface morphology of pyrite and the chemical species of sulfur and iron was discussed.

2. Materials and methods

2.1. Preparation and characterization of sample

To eliminate interference of impurities, pure pyrite crystal is used but not refractory gold ore in this experiment. The pyrite slice is prepared by the natural pyrite crystal obtained from a pyrite deposit in Yunnan, China. The pyrite powder ground to a particle size of less than 200 meshes. The pyrite crystals are cut into pieces having a thickness of 3 mm and then polished to a smooth surface using 2000 mesh sandpaper. The chemical reagents used in this experiment were analytical grade (hydrogen peroxide, potassium thiocyanate). The XRD and SEM image of the prepared pyrite slice and pyrite powder is shown in Fig. 1. It could be seen that the pyrite slice surface is very smooth in SEM images. The purity of prepared pyrite powder is 99.3%.

The experiments apparatus consists of an ultrasonic generator and a thermostat in Fig. 2. The pyrite slice is stabilized by
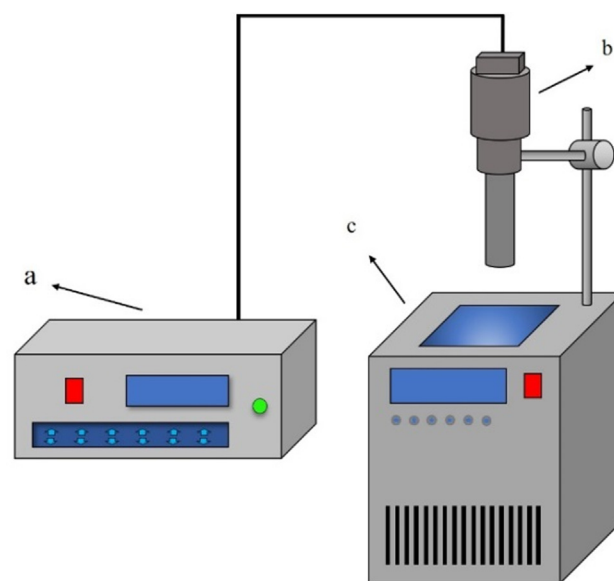
Fig. 2 Experiments apparatus (a) ultrasonic generator autocontroller; (b) ultrasonic generator probe; (c) thermostatic waterbath.
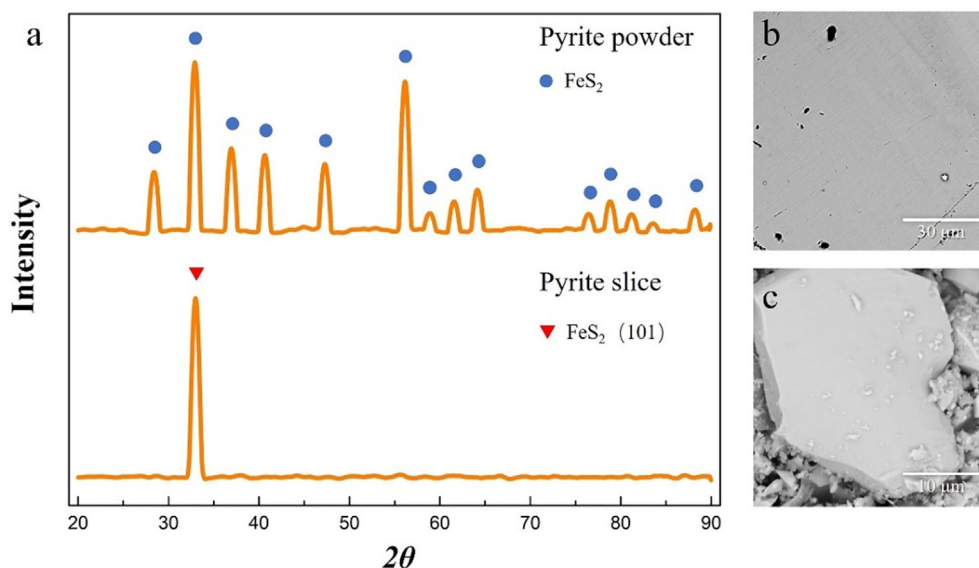
Fig. 1 XRD(a) and SEM(b, c) image of the prepared pyrite slice and pyrite powder.

waxing and the deionized water used in the experiment is deoxidized by argon aeration about 30 min before ultrasonic experiment.

2.2. Ultrasonic experiment

In oxidation experiment, the ultrasound power is set to 250 W, the distance between pyrite surface and ultrasound probe is 3 cm(the probe is 3 cm higher than the bottom of beaker), the temperature is controlled by thermostatic waterbath. After 4 h oxidation, the processed solid and liquid are collected respectively.

2.3. Sample characterization

The crystal structure of pyrite is characterized by XRD (X'Pert3powder, Panaco, Netherlands). The elemental valence of pyrite slice surface is characterized by X-ray photoelectron spectroscopy (XPS, K-Alpha, American). The surface morphology of pyrite slice is characterized by scanning electron microscope (Phenom ProX, Phenom-World, Netherlands). The chemical form and concentration of sulfur are determined by HPLC (LC2010plus, Japan). The chemical form of iron is determined by qualitative chemical analysis (using hydrogen peroxide and potassium rhodanide) and its concentration of iron is determined by inductively coupled plasma mass spectrometry (ICP-MS 7700x, American). pH meter (PHS-3S, Shanghai) is used to detect changes of H^+ ion after ultrasonic oxidation.

3. Results and discussion

3.1. The analysis of pyrite surface

3.1.1. The microstructure of pyrite

In this section, the microstructure of pyrite slice and powder is analyzed. Before ultrasonic treatment, the pyrite slice surface is smooth and with no scratch (Fig. 3a). after 4 h' ultrasonic treatment at 5 °C in deionized water, the pyrite slice is seriously corroded (Fig. 3b). Not only that, pyrite particle has integrity crystal structure before ultrasonic treatment (Fig. 3c), compared with severely corroded pyrite particle after ultrasound which crystal structure is severely damaged (Fig. 3d). This indicates that ultrasound has the ability to break the gold inclosure (pyrite).

In order to investigate the influences of different treatment condition on pyrite surface, several experiments are conducted to determine the influences of time, ultrasonic power, alkalinity and temperature, and the experiment results is shown in Fig. 4. It could be seen that the pyrite slice has a very smooth surface before ultrasonic treatment under SEM (Fig. 4a). With the increase of the ultrasonic power and temperature, the sur-
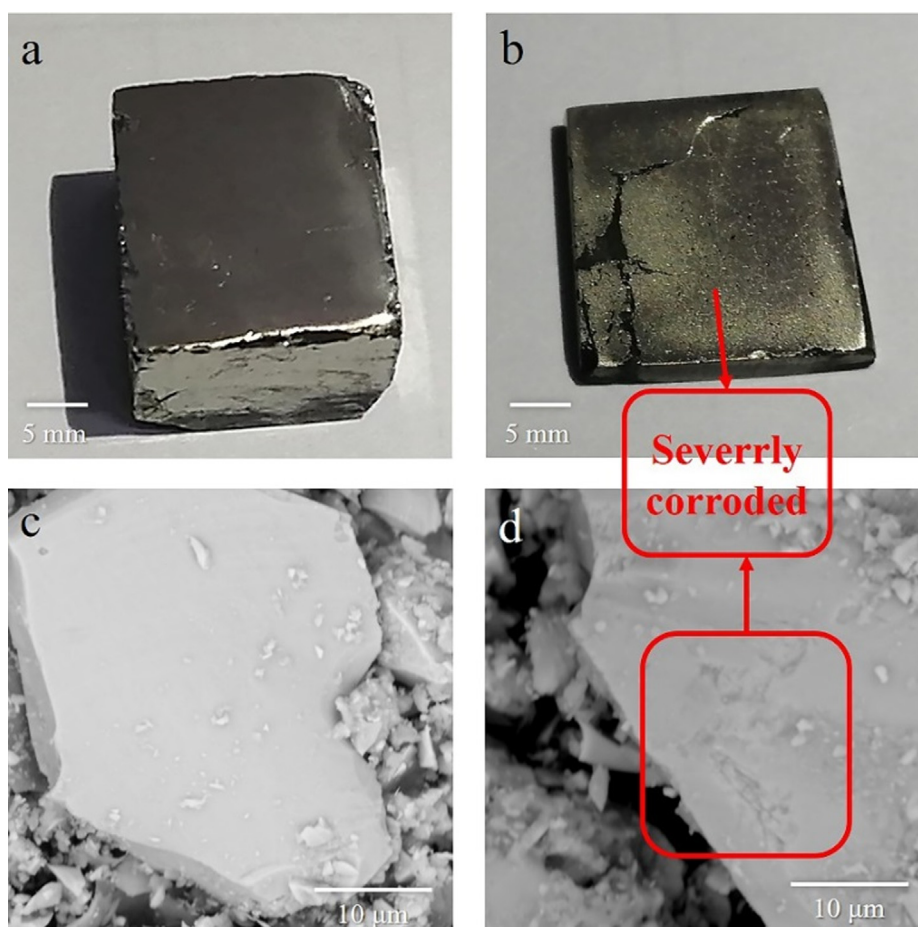

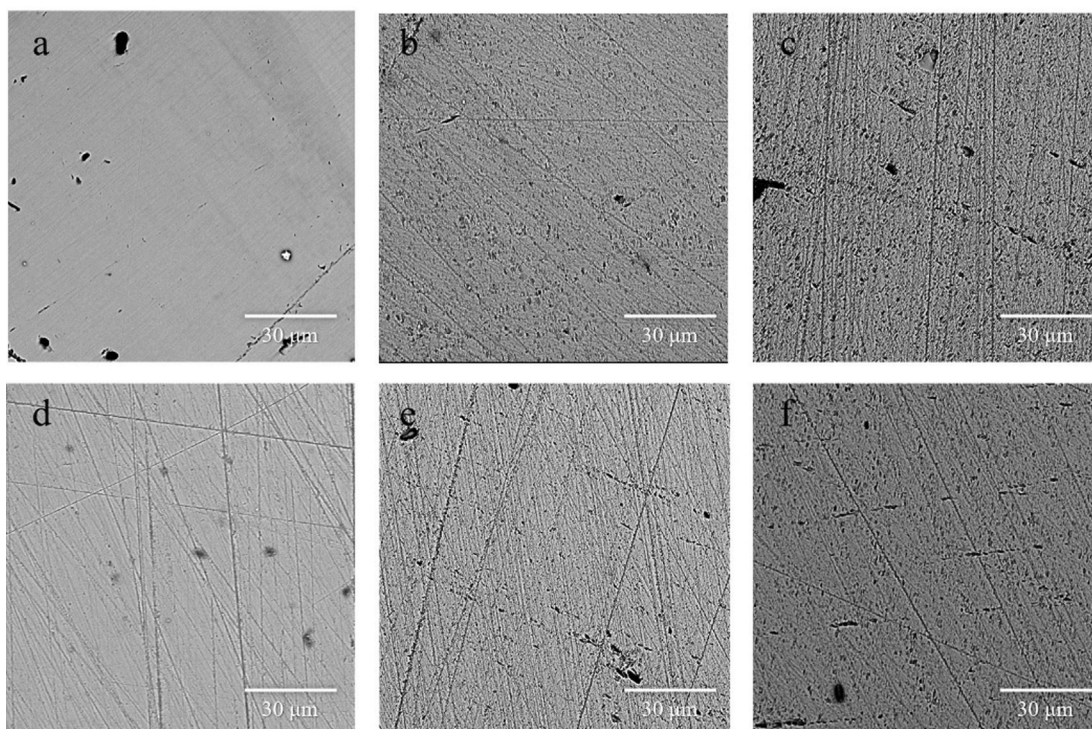**Fig. 3** The images of pyrite slice and pyrite powder before(a,c) and after ultrasound(250 W) for 4 h (b,d).

Fig. 4 SEM of the polished pyrite slice before (a) and after ultrasound at different condition. (Condition: (b)$T = 5^{\circ}$C, $W_U = 250W$, **t = 1 h**, $C_{NaOH} = 0mol/L$; (c) $T = 5^{\circ}$C, $W_U = 250W$, **t = 4 h**, $C_{NaOH} = 0mol/L$; (d) $T = 5^{\circ}$C, $W_U = 50W$, t = 4 h, $C_{NaOH} = 0mol/L$; (e) $T = 5^{\circ}$C, $W_U = 250W$, t = 4 h, $C_{NaOH} = 0.5mol/L$; (f) $T = 80^{\circ}$C, $W_U = 250W$, t = 4 h, $C_{NaOH} = 0.5mol/L$.)
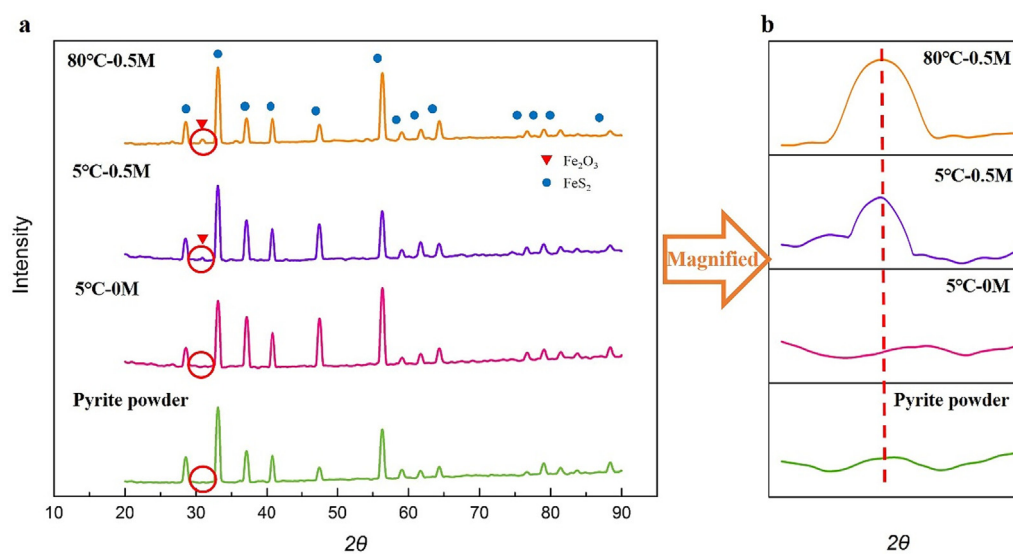

Fig. 5 (a) XRD image of pyrite powder before and after ultrasound; (b) partial magnified XRD image of pyrite powder before and after ultrasound.

face corrosion of pyrite becomes also more and more obvious (Fig. 4d and c). This result indicates that ultrasound can effectively damage pyrite structure under neutral condition. The increases of alkalinity have slightly improvement on pyrite corrosion (Fig. 4e and f). The EDS analysis indicates that some oxidant have formed on the pyrite surface under alkaline condition after ultrasound (**Fig. S1** and **Fig S2**). The hematite or

feroxyhite could be the oxidant base on previous study (Caldeira et al., 2003).

3.1.2. The chemical changes of pyrite surface

In this section, XRD and XPS were used to determine the chemical changes of pyrite powder and slices, respectively. The oxidized pyrite powder after drying was analyzed by
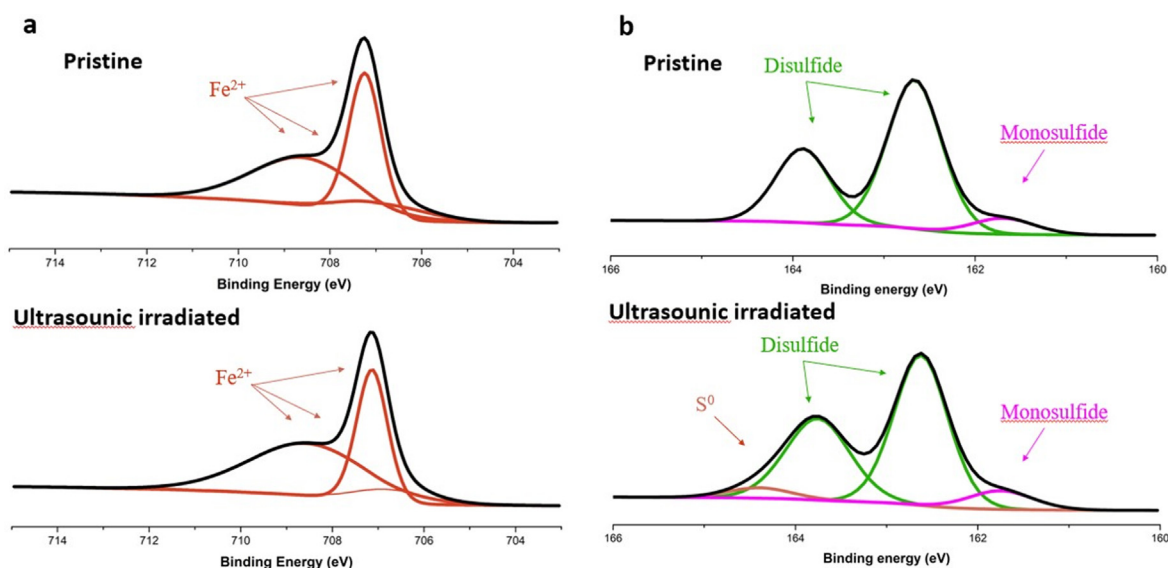
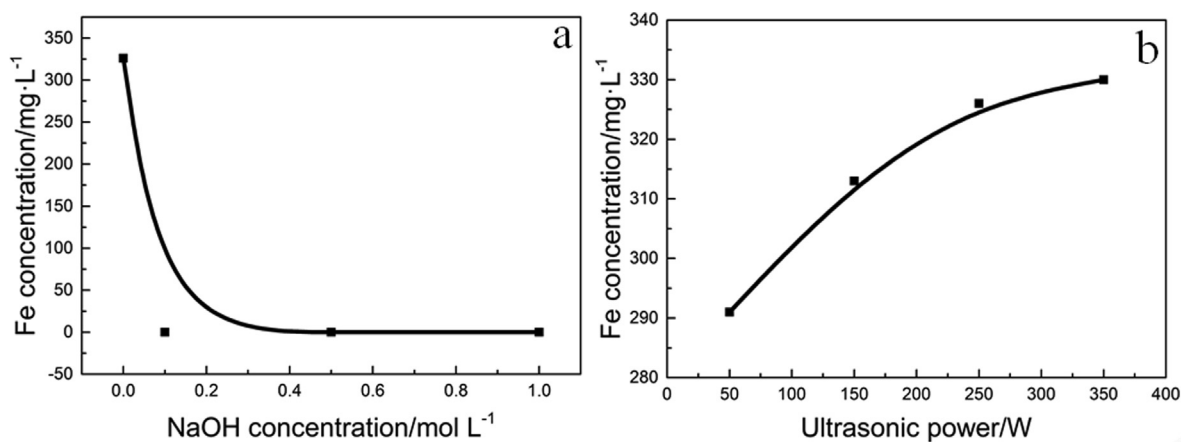Fig. 6 XPS spectra of iron(a) and sulfur(b) of pyrite slices.

Fig. 7 Effect of NaOH concentration and ultrasonic power on the iron concentration in the solution. (Conditions: (a) $T = 5°C$, $W_U = 250W$; (b) $T = 5°C$, $C_{NaOH} = 0mol/L$).

XRD (Fig. 5). Under neutral condition, no new phases appear. However, Fe_2O_3 were detected in the dried slag when alkalinity or temperature rises (Fig. 5(b)). The formation of iron oxide under alkalinity or high temperature condition might attribute to the hydrolyzation of iron ion produced by pyrite (Caldeira et al., 2003). The ultimate product of iron oxide(Fe_2O_3) might be formed by hematite or feroxyhyte (Caldeira et al., 2003).

Fig. 6 indicates the Fe2p and S2p core level spectra of the polished pyrite slice surface before and after ultrasound. The three multiplet peaks at 706.7 eV ($Fe2p_{3/2A}$), 707.6 eV ($Fe2p_{3/2B}$) and 708.6 eV ($Fe2p_{3/2C}$) correspond to high spin Fe(II) ions bonded to sulfur (Fig. 6a) (Demoisson et al., 2007). The spectrum of sulfur has two main peak at 163.8 eV($S2p_{1/2}$) and 162.6 eV($S2p_{3/2}$), which indicate the presence of disulfide (Fig. 6b) (Demoisson et al., 2007; Liao et al., 2013; Scheinost et al., 2008; Thomas et al., 2003). The small peak at 161.7 eV($S2p_{3/2}$) contribute to monosulfide (Demoisson et al., 2007). After ultrasound for 4 h, the multiplet peaks of Fe(II) ions barely changed and there is a new
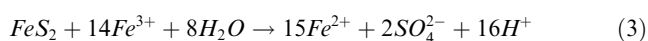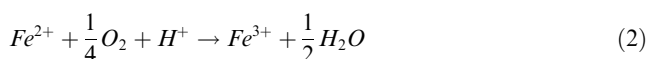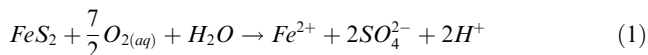
peak at 164.4 eV in the spectrum of sulfur, which attribute to elemental sulfur (Demoisson et al., 2007). This is due to that pyrite decomposes to ferric ion and elemental sulfur in the presence of oxidizer.

3.2. Effect of ultrasonic cavitation on the ion species

3.2.1. The iron species distribution

ICP and qualitative chemical analysis was used to determine the concentration of iron ions in solution. The saturated potassium thiocyanate solution (KSCN) and hydrogen peroxide (H_2O_2) was used to determine the chemical valence of iron ions (Video.1). It is obvious that few Fe(III) existed in liquid, because the color barely changed after adding KSCN. Oppositely, when H_2O_2 was firstly added, the liquid became blood red instantly after adding KSCN. Which proved that the iron was mainly existed as Fe(II), few are in the form of Fe(III). It has been reported that the oxidation of pyrite in aqueous solution is mainly carried out through the following chemical

reactions(Eq1-3) (Caldeira et al., 2003; Garrels and Thompson, 1960; Singer and Stumm, 1970). This also suggests that Fe(II) is the dominant species in the solution. Further experiment indicated that iron ions were only existed at neutral condition, the Fe(II) ions deposited when the NaOH concentration was raised (Fig. 7a). This is contributed to hydrolyzation of Fe(II) ion (Caldeira et al., 2003). This result is coordinate with XRD analysis from Section 3.1.1. The Fe(II) concentration will increase as the power increases (Fig. 7b). A higher ultrasonic power can motivate stronger cavitation, strip the deposited iron oxide and expose the new reaction interface, which promotes the oxidation of pyrite (Ince et al., 2001; Villeneuve and Alberti, 2009).

$$FeS_2 + \frac{7}{2}O_{2(aq)} + H_2O \rightarrow Fe^{2+} + 2SO_4^{2-} + 2H^+ \quad (1)$$

$$Fe^{2+} + \frac{1}{4}O_2 + H^+ \rightarrow Fe^{3+} + \frac{1}{2}H_2O \quad (2)$$

$$FeS_2 + 14Fe^{3+} + 8H_2O \rightarrow 15Fe^{2+} + 2SO_4^{2-} + 16H^+ \quad (3)$$

3.2.2. Sulfur species distribution in water

Fig. 8 a is the image of HPLC of the sulfur species. From Fig. 8a, only SO_4^{2-} and $S_2O_3^{2-}$ were detected, no other sulfur ions are detected (S^{2-}, SO_3^{2-}, polysulfide, etc.). This result indicates that pyrite will only be oxidized to SO_4^{2-} and $S_2O_3^{2-}$ under ultrasound. More specific experiment was conducted to determine the influences of different reaction condition. Fig. 8 (b to d) is the effect of NaOH concentration, temperature and ultra-

sonic power on the sulfur species. Under ultrasound (250 W) for 4 h at 5 °C (Fig. 8b), the SO_4^{2-} and $S_2O_3^{2-}$ concentration increases significantly after adding NaOH, but decreases when NaOH concentration is too high. This result indicates pyrite oxidation is in mild alkalinity under ultrasound. Moreover, the concentration of $S_2O_3^{2-}$ under alkaline condition is much higher than neutral condition, which is contributed to a higher stability of $S_2O_3^{2-}$ under alkaline condition (Aylmore and Muir, 2001; Ha et al., 2014). Because the cavitation effect increases along with ultrasonic power, the oxidation ability of the system increased (Villeneuve and Alberti, 2009; Hu et al., 2008). The concentration of SO_4^{2-} and $S_2O_3^{2-}$ increases along with ultrasonic power (Fig. 8d, conditions: $C_{NaOH} = 0M$, temperature = 5 °C). The SO_4^{2-} and $S_2O_3^{2-}$ concentration decreases tremendously when temperature rises (Fig. 8c, condition: $C_{NaOH} = 0.5mol/L$, $W_U = 250W$). This might contribute to hydrolyzation of iron ions which diminished the oxidation ability. The effect of temperature shows that the oxidation of pyrite under ultrasound should be carried out at low temperature.

3.2.3. pH changes under ultrasonic cavitation

The changes of H^+ concentration under ultrasound were measured by pH meter. Fig. 9a indicated the increases of ultrasonic power could significantly increase H^+ concentration (initial pH = 7). This is due to the decomposition of H_2O into the hydrogen and hydroxyl radicals under ultrasonic treatment. The hydroxyl radicals participate in the pyrite oxidation. The oxidation of pyrite under ultrasound is a reaction that releases hydrogen ions. Based on the previous analysis, the chemical
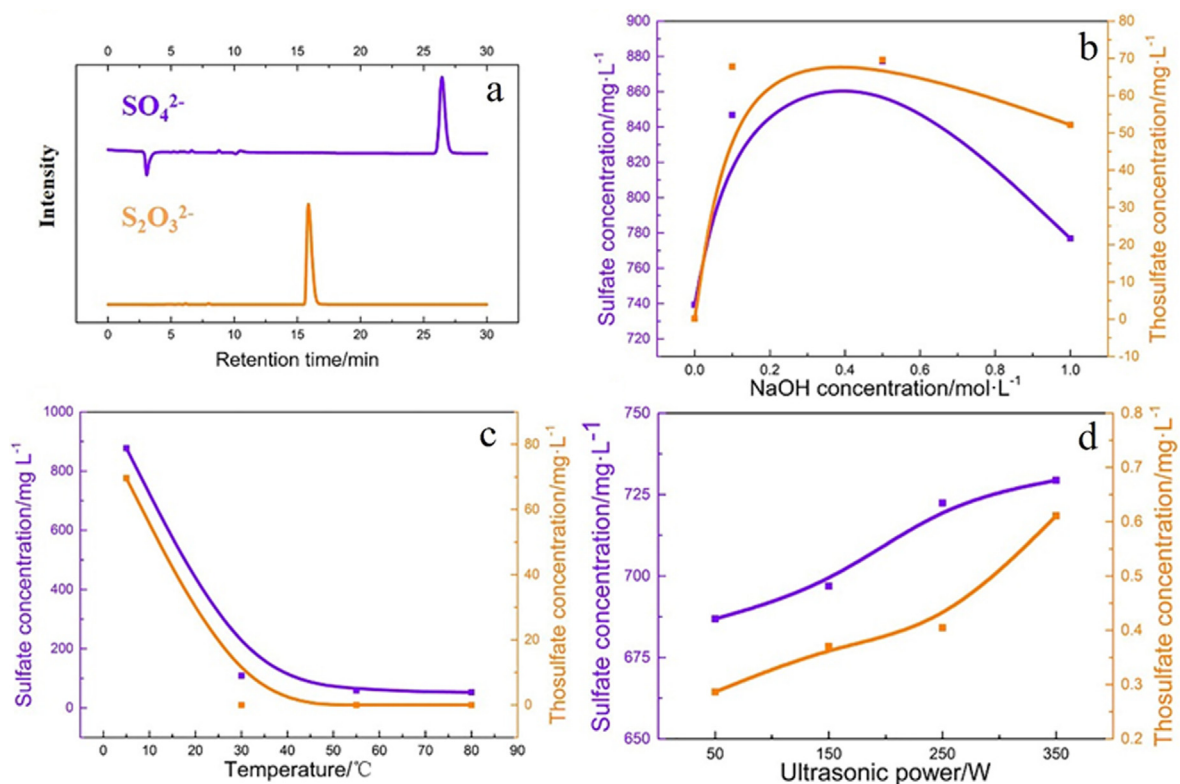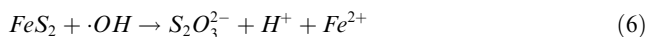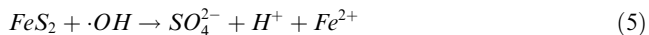

Fig. 8 The image of HPLC of the sulfur species(a), Effect of NaOH concentration(b), temperature(c) and ultrasonic power(d) on the sulfur species.

reaction of pyrite oxidation under ultrasound should be carried out as follow:

$$H_2O \rightarrow \cdot H + \cdot OH \tag{4}$$

$$FeS_2 + \cdot OH \rightarrow SO_4^{2-} + H^+ + Fe^{2+} \tag{5}$$

$$FeS_2 + \cdot OH \rightarrow S_2O_3^{2-} + H^+ + Fe^{2+} \tag{6}$$

This result consists with previous analysis, which proved that ultrasound could oxidize pyrite effectively. The hydrogen radicals might also formats as hydrogen accord as Draganic's study (Draganic and Draganic, 1971). The pH changes of each experiment are shown in **Table S1**; **Table S2** and **Table S3**. It could be seen that under neutral condition (**Fig. 9b**, **Table. S2**), the pH after ultrasonic oxidation decreases significantly. However, the changes of the final pH decrease rapidly with the rises of the initial pH. This result is similar with the change of sulfur and iron species, which proved that oxidation was
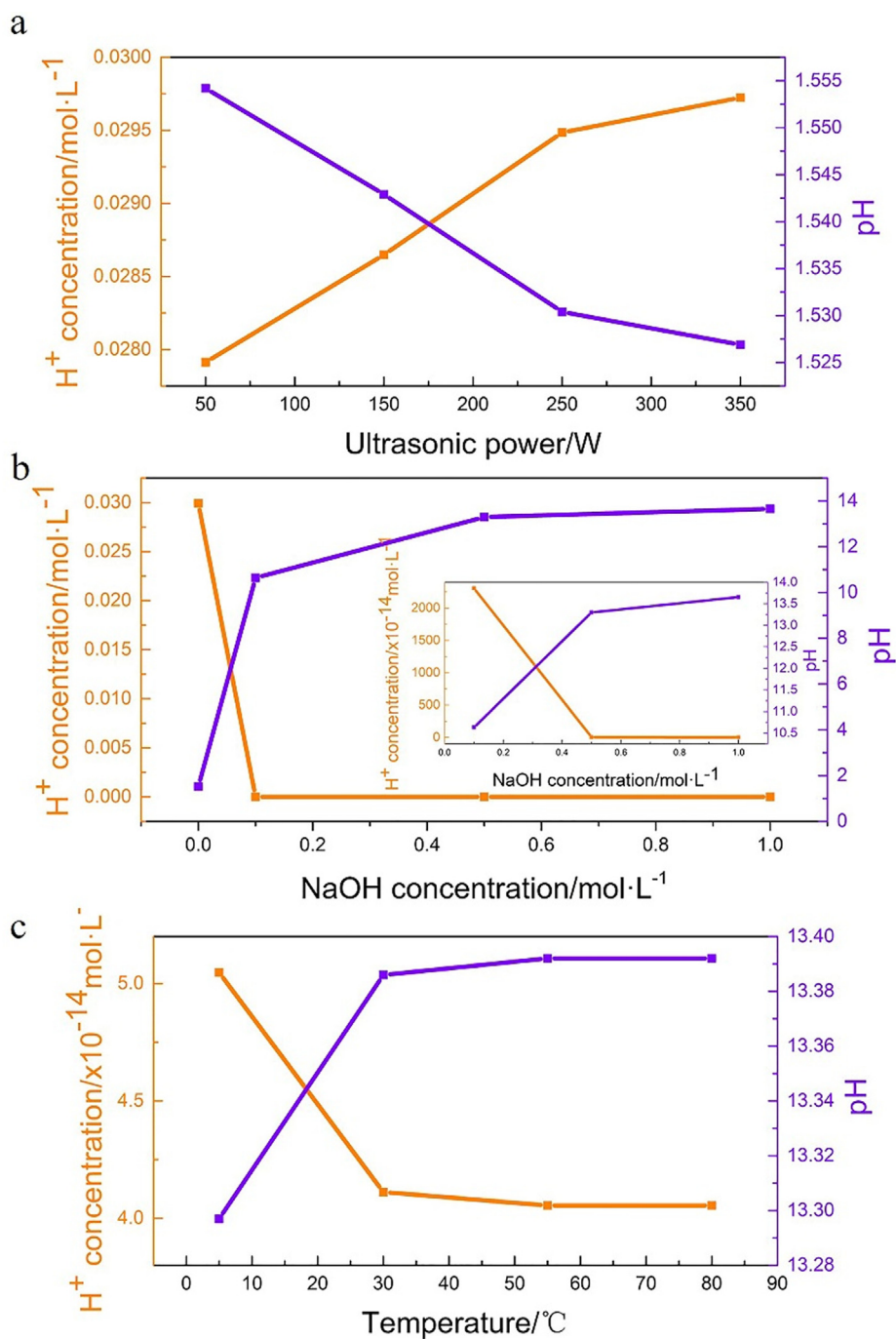

Fig. 9 pH changes after ultrasonic oxidation under different condition. (condition: (a) $T = 5°C$, $C_{NaOH} = 0 mol/L$; (b) $T = 5°C$, $W_U = 250W$; (c) $W_U = 250W$, $C_{NaOH} = 0.5 mol/L$;).
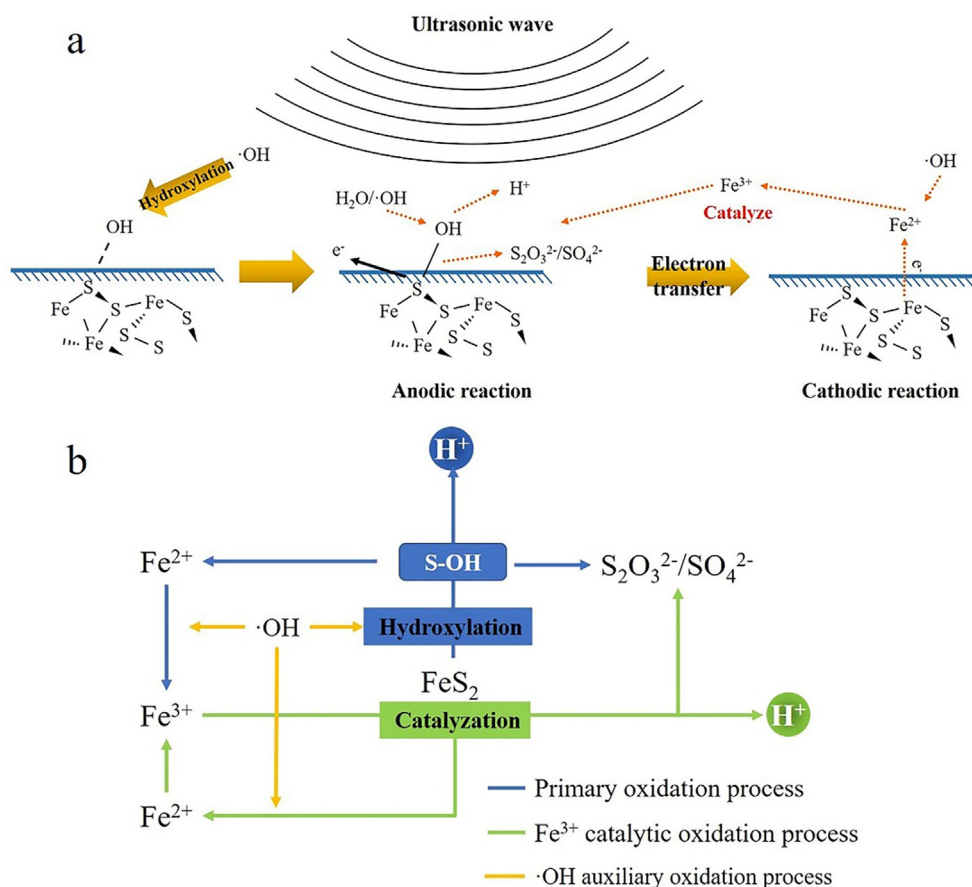
Fig. 10 (a) the oxidation mechanism of pyrite under ultrasonic cavitation; (b) Migration diagram of elements during pyrite oxidationBase on pyrite oxidation mechanism under ultrasound, the utilization of ultrasonic pretreatment in refractory gold ore is a promising technology. It could be an environmental-friendly and low cost way to improving gold recovery rate in refractory gold ore. Meanwhile, the application of ultrasonic treatment combined with traditional methods, such as chemical oxidation pretreatment or high-pressure oxidation pretreatment (Li et al., 2009; Shaoluan et al., 1997; Nunan et al., 2017), could also improve pretreatment result which enhanced gold leaching.

weakened with the increase of the initial alkalinity. Under 0.5 M NaOH, the pH hardly changed after temperature rises (Fig. 9c, Table.S3). This indicates the rises of temperature have slightly influences to ultrasonic oxidation.

3.3. The oxidation mechanism of pyrite under ultrasound

The oxidation mechanism of pyrite has been studied for several years (Demoisson et al., 2007; Holmes and Crundwell, 2000; Herman; Chandra and Gerson, 2010; McKibben and Barnes, 1986; Holmes and Crundwell, 2000). Fe^{3+} and O_2 are considered as the most important oxidant during pyrite oxidation process (McKibben and Barnes, 1986; Holmes and Crundwell, 2000; Herman; Nicholson et al., 1988). Herman (Holmes and Crundwell, 2000) and McKibben (McKibben and Barnes, 1986) points out that Fe^{3+} has more aggressive effect on pyrite oxidation than O_2, even at higher pH where Fe^{3+} may hydrolyze. In previous section, the oxidation extent of pyrite is closely related to the concentration of iron ions in the solution. The higher the iron ions concentration, the higher the oxidation of pyrite. However, under ultrasound, the decomposition of water produces strongly oxidizing free radi-

cals, no Fe^{3+} or O_2 exists as oxidant. The only oxidant in this system is hydroxyl radical generated by ultrasonic cavitation (Rooze et al., 2013; Feng et al., 2002; Shchukin et al., 2011). In ultrasonic field, hydroxyl radical ($\cdot OH$) can be motivated by acoustic cavitation (Rooze et al., 2013; Entezari and Kruus, 1996; Entezari and Kruus, 1994). The $\cdot OH$ has very strong oxidizing property. The redox potential of $\cdot OH$ is 2.80 V, which is much higher than Fe ion and O_2 ($E_{Fe^{3+}/Fe^{2+}} = 0.73v$, $E_{O_2} = 1.23v$). When Fe^{3+}/Fe^{2+} diffuses into the solution, it will become a catalyst for pyrite oxidation (eq.3 and 7). This is the main reason that the iron in the solution is mainly in the form of Fe^{2+}. Based on recent research (Demoisson et al., 2007; Holmes and Crundwell, 2000; Herman; Nicholson et al., 1988; Entezari and Kruus, 1996; Entezari and Kruus, 1994; Rooze et al., 2013), the oxidation mechanism of pyrite under ultrasonic cavitation can be summarized as follow. Under ultrasonic cavitation, the pyrite surface will be hydroxylated by hydroxyl radicals primarily. After that, more $\cdot OH$ or H_2O will interact with hydroxy for further anodic reaction. The SO_4^{2-}, $S_2O_3^{2-}$ and H^+ releases with electron transfer. Meanwhile, the iron will dissolve into water in the form of Fe^{2+}. The Fe^{2+} will further be oxidized to Fe^{3+} by hydroxyl radicals. More importantly, the occurrence of

Fe^{3+}/Fe^{2+} oxidation–reduction couples can further accelerate the oxidation of pyrite under ultrasonic cavitation based on previous analysis. The oxidation mechanism of pyrite under ultrasonic cavitation and migration diagram of elements can be summarized as Fig. 10.

$$Fe^{2+} + \cdot OH \rightarrow Fe^{3+} + OH^- \tag{7}$$

4. Conclusion

The aim of present paper was to investigate the oxidation mechanism of pyrite under ultrasound and neutral condition. A promising pretreatment method for refractory gold ore with low cost and free of contamination was provided. The founding of this paper can be summarized as follows:

1) Pyrite surface was severely damaged into cracks and pores by ultrasound. This proved that ultrasound could be an effective way to expose gold from pyrite enclosure.
2) Under free oxygen condition, the oxidation of pyrite is initiated by hydroxyl radical. The oxidation rate is determined by cavitation efficiency. The increases of ultrasonic power can effectively accelerate pyrite oxidation, which promote gold exposure from pyrite enclosure.
3) The oxidation rate is highly dependent on pH at alkaline condition, which accelerates the formation of hydroxide of iron. Temperature shares the same effect with pH.
4) The oxidation of pyrite will release a lot of hydrogen ions, especially in neutral pH.

CRediT authorship contribution statement

Qihao Gui: Conceptualization, Methodology, Validation, Formal analysis, Investigation, Writing - Original Draft, Writing - Original Draft, Visualization. **Shixing Wang:** Conceptualization, Methodology, Validation, Resources, Writing - Original Draft, Visualization, Supervision, Project administration, Funding acquisition. **Libo Zhang:** Conceptualization, Methodology, Resources, Supervision, Project administration, Funding acquisition.

Declaration of Competing Interest

The authors declare that they have no known competing financial interests or personal relationships that could have appeared to influence the work reported in this paper.

Acknowledgment

References

Fraser, K.S., Walton, R.H., Wells, J.A., 1991. Processing of refractory gold ores. Miner. Eng. 4, 1029–1041. https://doi.org/10.1016/0892-6875(91)90081-6.

Boboev, I.R., Strizhko, L.S., Bobozoda, Sh., Gorbunov, E.P., 2016. Kinetic investigation of sulfidizing annealing of scorodite in processing of refractory oxidized gold-containing ores. Russ. Metall. 2016, 171–173. https://doi.org/10.1134/S0036029516030046.

Fomchenko NV, Kondrat'eva TF, Muravyov MI. A new concept of the biohydrometallurgical technology for gold recovery from refractory sulfide concentrates. Hydrometallurgy 2016;164:78–82. https://doi.org/10.1016/j.hydromet.2016.05.011.

Li, Q., Li, D., Qian, F., 2009. Pre-oxidation of high-sulfur and high-arsenic refractory gold concentrate by ozone and ferric ions in acidic media. Hydrometallurgy 97, 61–66. https://doi.org/10.1016/j.hydromet.2009.01.002.

Liu, X., Li, Q., Zhang, Y., Jiang, T., Yang, Y., Xu, B., et al, 2019. Improving gold recovery from a refractory ore via Na_2SO_4 assisted roasting and alkaline Na_2S leaching. Hydrometallurgy 185, 133–141. https://doi.org/10.1016/j.hydromet.2019.02.008.

Ofori-Sarpong, G., Osseo-Asare, K., Tien, M., 2011. Fungal pretreatment of sulfides in refractory gold ores. Miner. Eng. 24, 499–504. https://doi.org/10.1016/j.mineng.2011.02.020.

Celep, O., Alp, İ., Deveci, H., 2011. Improved gold and silver extraction from a refractory antimony ore by pretreatment with alkaline sulphide leach. Hydrometallurgy 105, 234–239. https://doi.org/10.1016/j.hydromet.2010.10.005.

Deschênes, G., Xia, C., Fulton, M., Cabri, L.J., Price, J., 2009. Evaluation of leaching parameters for a refractory gold ore containing aurostibite and antimony minerals: Part I - Central zone. Miner. Eng. 22, 799–808. https://doi.org/10.1016/j.mineng.2009.02.003.

Šíma, V., Kratochvíl, P., Kozelský, P., Schindler, I., Hána, P., 2009. FeAl-based alloys cast in an ultrasound field. IJMR 100, 382–385. https://doi.org/10.3139/146.110041.

Xin W, Srinivasakannan C, Xin-hui D, Jin-hui P, Da-jin Y, shao-hua J. Leaching kinetics of zinc residues augmented with ultrasound. Separation and Purification Technology 2013;115:66–72. https://doi.org/10.1016/j.seppur.2013.04.043.

Luque-García JL, Luque de Castro MD. Ultrasound: a powerful tool for leaching. TrAC Trends in Analytical Chemistry 2003;22:41–7. https://doi.org/10.1016/S0165-9936(03)00102-X.

Verdan, S., Burato, G., Comet, M., Reinert, L., Fuzellier, H., 2003. Structural changes of metallic surfaces induced by ultrasound. Ultrason. Sonochem. 10, 291–295. https://doi.org/10.1016/S1350-4177(03)00106-8.

Zhang, G., Wang, S., Zhang, L., Peng, J., 2016. Ultrasound-intensified Leaching of Gold from a Refractory Ore. ISIJ Int. 56, 714–718. https://doi.org/10.2355/isijinternational.ISIJINT-2015-476.

Rooze, J., Rebrov, E.V., Schouten, J.C., Keurentjes, J.T.F., 2013. Dissolved gas and ultrasonic cavitation – A review. Ultrason. Sonochem. 20, 1–11. https://doi.org/10.1016/j.ultsonch.2012.04.013.

Ishihara, N., Doi, Y., Hirabayashi, H., Ishii, T., Kita, I., Negishi, K., et al, 1975. Fundamental Study of Ultrasonic Hydrogen Bubble Chamber by Measurement of Cavitation Threshold. Jpn J. Appl. Phys. 14, 101–112. https://doi.org/10.1143/JJAP.14.101.

Feng, R., Zhao, Y., Zhu, C., Mason, T.J., 2002. Enhancement of ultrasonic cavitation yield by multi-frequency sonication. Ultrason. Sonochem. 9, 231–236. https://doi.org/10.1016/S1350-4177(02)00083-4.

Shchukin, D.G., Skorb, E., Belova, V., Möhwald, H., 2011. Ultrasonic Cavitation at Solid Surfaces. Adv. Mater. 23, 1922–1934. https://doi.org/10.1002/adma.201004494.

Wang, Q.-Y., Bai, S.-L., Liu, Z.-D., 2014. Study on Cavitation Erosion-Corrosion Behavior of Mild Steel under Synergistic Vibration Generated by Ultrasonic Excitation. Tribol. Trans. 57, 603–612. https://doi.org/10.1080/10402004.2014.890264.

Caldeira, C.L., Ciminelli, V.S.T., Dias, A., Osseo-Asare, K., 2003. Pyrite oxidation in alkaline solutions: nature of the product layer. Int. J. Miner. Process 14.

Demoisson, F., Mullet, M., Humbert, B., 2007. Investigation of pyrite oxidation by hexavalent chromium: Solution species and surface

chemistry. J. Colloid Interf. Sci. 316, 531–540. https://doi.org/10.1016/j.jcis.2007.08.011.

Liao, F., Świątowska, J., Maurice, V., Seyeux, A., Klein, L.H., Zanna, S., et al, 2013. Electrochemical lithiation and passivation mechanisms of iron monosulfide thin film as negative electrode material for lithium-ion batteries studied by surface analytical techniques. Appl. Surf. Sci. 283, 888–899. https://doi.org/10.1016/j.apsusc.2013.07.039.

Scheinost, A.C., Kirsch, R., Banerjee, D., Fernandez-Martinez, A., Zaenker, H., Funke, H., et al, 2008. X-ray absorption and photoelectron spectroscopy investigation of selenite reduction by FeII-bearing minerals. J. Contam. Hydrol. 102, 228–245. https://doi.org/10.1016/j.jconhyd.2008.09.018.

Thomas JE, Skinner WM, Smart RS t. C. A comparison of the dissolution behavior of troilite with other iron(II) sulfides; implications of structure. Geochimica et Cosmochimica Acta 2003;67:831–43. https://doi.org/10.1016/S0016-7037(02)01146-8.

Garrels, R.M., Thompson, M.E., 1960. Oxidation of pyrite by iron sulfate solutions.pdf. Am. J. Sci. 258-A, 57–67.

Singer, P.C., Stumm, W., 1970. Acidic Mine Drainage: The Rate-Determining Step. Science 167, 1121–1123.

Ince, N.H., Tezcanli, G., Belen, R.K., Apikyan, İ.G., 2001. Ultrasound as a catalyzer of aqueous reaction systems: the state of the art and environmental applications. Appl. Catal. B 29, 167–176. https://doi.org/10.1016/S0926-3373(00)00224-1.

Villeneuve, L., Alberti, L., 2009. Assay of hydroxyl radicals generated by focused ultrasound. Ultrason. Sonochem. 6.

Aylmore, M.G., Muir, D.M., 2001. Thiosulfate leaching of gold—A review. Miner. Eng. 14, 135–174. https://doi.org/10.1016/S0892-6875(00)00172-2.

Ha VH, Lee J, Huynh TH, Jeong J, Pandey BD. Optimizing the thiosulfate leaching of gold from printed circuit boards of discarded mobile phone 2014:9.

Hu, Y., Zhang, Z., Yang, C., 2008. Measurement of hydroxyl radical production in ultrasonic aqueous solutions by a novel chemilumi-

nescence method. Ultrason. Sonochem. 15, 665–672. https://doi.org/10.1016/j.ultsonch.2008.01.001.

Draganic, I.G., Draganic, Z.D., 1971. The radiation chemistry of water. ACADEMIC PRESS, American.

Chandra, A.P., Gerson, A.R., 2010. The mechanisms of pyrite oxidation and leaching: A fundamental perspective. Surf. Sci. Rep. 65, 293–315. https://doi.org/10.1016/j.surfrep.2010.08.003.

McKibben, M.A., Barnes, H.L., 1986. Oxidation of pyrite in low temperature acidic solutions: Rate laws and surface textures. Geochim. Cosmochim. Acta 50, 1509–1520. https://doi.org/10.1016/0016-7037(86)90325-X.

Holmes, P.R., Crundwell, F.K., 2000. The kinetics of the oxidation of pyrite by ferric ions and dissolved oxygen: an electrochemical study. Geochim. Cosmochim. Acta 64, 263–274. https://doi.org/10.1016/S0016-7037(99)00296-3.

Herman JS. Pyrite oxidation at chumneutral pH n.d.:12.

Nicholson, R.V., Gillham, R.W., Reardon, E.J., 1988. Pyrite oxidation in carbonate-buffered solution: 1. Experimental kinetics. Geochim. et Cosmochimica Acta 52, 1077–1085. https://doi.org/10.1016/0016-7037(88)90262-1.

Entezari, M.H., Kruus, P., 1996. Effect of frequency on sonochemical reactions II. Temperature and intensity effects. Ultrasonics Sonochem. 3, 19–24. https://doi.org/10.1016/1350-4177(95)00037-2.

Entezari MH, Kruus P. Effect of frequency on sonochemical reactions. I: Oxidation of iodide. Ultrasonics Sonochemistry 1994;1:S75–9. https://doi.org/10.1016/1350-4177(94)90001-9.

Shaoluan, Zhou, Quanqing, Sun, Xiaohong, Zhang, Xin, Li, 1997. Pressure leaching technology of refractoryt gold ore. Uranium Min. Metallurgy 16, 237–244.

Nunan, T.O., Viana, I.L., Peixoto, G.C., Ernesto, H., Verster, D.M., Pereira, J.H., et al, 2017. Improvements in gold ore cyanidation by pre-oxidation with hydrogen peroxide. Miner. Eng. 108, 67–70. https://doi.org/10.1016/j.mineng.2017.01.006.